J. Vis. Commun. Image R. 20 (2009) 323–338

Contents lists available at ScienceDirect

J. Vis. Commun. Image R.

journal homepage: www.elsevier.com/locate/jvci

A visible watermarking algorithm based on the content and contrast aware (COCOA) technique

Min-Jen Tsai *

National Chiao Tung University, Institute of Information Management, 1001 Ta-Hsueh Road, Hsin-Chu 300, Taiwan, ROC

ARTICLE INFO

Article history:
Received 13 June 2008
Accepted 31 March 2009
Available online 17 April 2009

Keywords:
CSF
Human Vision System
NVF
Visible watermarking
Wavelet transform
Copyright protection
Image inpainting
Image recovery

ABSTRACT

A novel visible watermarking algorithm based on the content and contrast aware (COCOA) technique with the consideration of Human Visual System (HVS) model is presented in this study. In order to determine the optimal watermark locations and strength at the watermark embedding stage, the COCOA visible watermarking utilizes the global and local characteristics of the host and watermark images in the discrete wavelet transform (DWT) domain. To achieve the best tradeoff between the embedding energy of watermark and the perceptual translucence, the utilization of contrast–sensitive function, noise visible function of perceptual model, and the basis function amplitudes of DWT coefficients are fine tuned, for the best quality of perceptual translucence and noise reduction of the COCOA algorithm. The experimental results demonstrate that COCOA technique not only provides high PSNR values for the watermarked images, but also preserves the watermark visibility under various signal processing operations, especially the watermark removal attack.

1. Introduction

Due to the advancement of digital technologies and rapid communication network deployment, a wide variety of multimedia contents have been digitalized and their distribution or duplication made easy without any reduction in quality through both authorized and unauthorized distribution channels. With the advantages of easy editing and reproduction of digitalized data, the protection of the intellectual rights and the authentication of digital multimedia no doubt have become issues of great importance in recent years.

Over the last two decades, software, multimedia, and all digital content-driven industries, whether on the Internet or not, have also come to rely on effective copyright protection, especially as a revolution is underway in digital entertainment and marketing. In the beginning, conventional encryption algorithms such as DES or RSA are directly adopted to protect digital media. In these cryptographic systems, only the valid users who have the correct decryption key can decrypt the encrypted content and use it. But once such content is decrypted and the users can duplicate or retransmit it repeatedly, the authors will have no way to track those digital data. Therefore, conventional cryptography is evidently not a good way to solve this problem.

Digital watermarking [1] has been extensively researched and regarded as a potentially effective means for protecting copyright of digital media in recent years, since it makes possible the embedding of secret information in the digital content to identify the copyright owner. Digital watermarking describes methods and technologies that allow hidden information, for example, a sequence of numbers or recognizable pattern in digital media, such as images, video and audio. Many different digital watermarking techniques have been proposed by a number of researchers, and these methods can be divided into various categories [2]. One important classification is to divide digital watermarking algorithms into visible and invisible ones according to the perceptivity of watermark data in watermarked contents. Since the visible watermarking schemes protect copyrights in a more active method, they not only prevent pirating but also recognize the copyright of multimedia data immediately. Digital contents embedded with visible watermarks will overlay recognizable but unobtrusive copyright patterns to identify its ownership. Therefore, a useful visible watermarking technique should retain all details of the contents, while ensuring that the embedded patterns are difficult or even impossible to be removed, so that no one could use watermarked data illegally. Thus this study will mainly focus on the research for visible watermarking techniques.

Regarding the digital watermarking techniques, Fig. 1(a) and (b) describes the generic structure for watermark embedding and extraction processes. First, a host image (original image) directly embeds watermark in spatial domain or is transformed into frequency domain through the well-known spread spectrum approach, i.e. DFT (discrete Fourier transform), DCT (discrete

* Fax: +1 886 3 572 3792.
E-mail addresses: mjtsai@cc.nctu.edu.tw, mjtsai@gmail.com.

1047-3203/$ - see front matter © 2009 Elsevier Inc. All rights reserved.
doi:10.1016/j.jvcir.2009.03.011

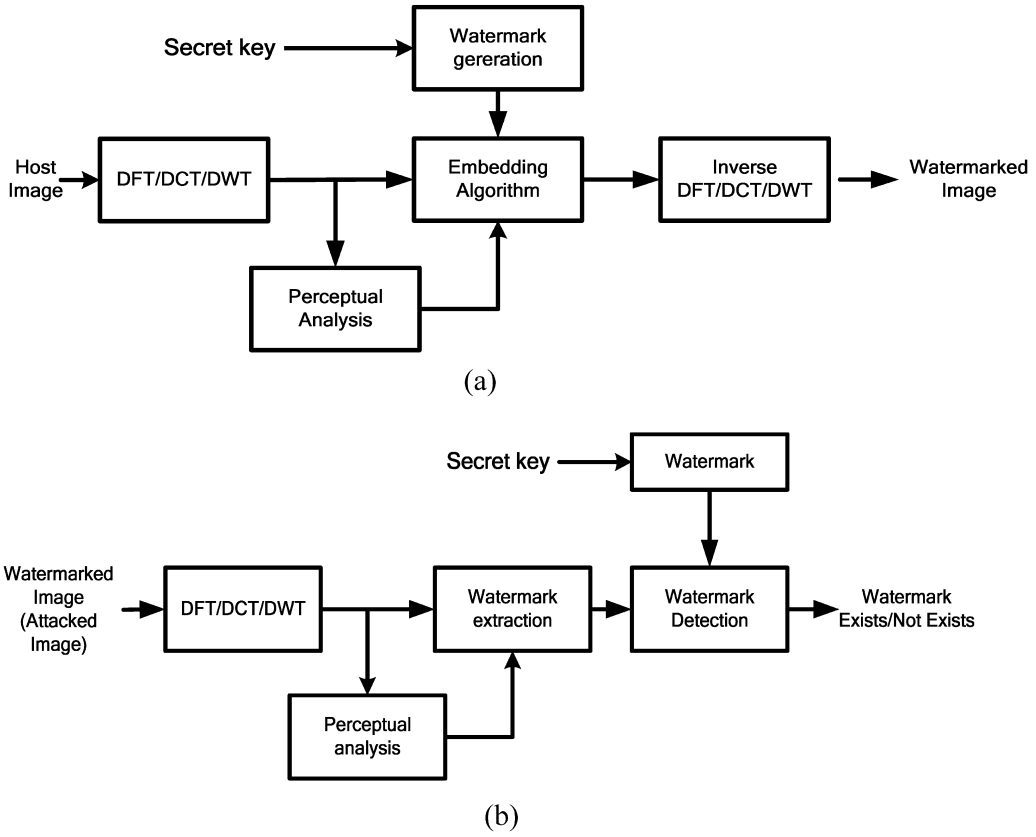

Fig. 1. (a) Watermark embedding process. (b) Watermark extraction process.

cosine transform) or DWT (discrete wavelet transform). However, the algorithms using transform domain approach develop more robust watermarking techniques than directly embedding watermark into the spatial domain. Consequently, coefficients are passed through a perceptual analysis block that determines how strong the watermark in embedding algorithm can be, so that the resulting watermarked image is acceptable. The secret key is applied to generate watermark and watermark embedding location. The watermark is embedded through using a well-designed algorithm based on mathematical or statistical model. If the host image is employed in frequency domain, the inverse spread spectrum approach is then adopted to obtain a watermarked image [1]. The watermark extraction applies to the similar operations in embedding processes. It employs the inverse operations or uses the mathematical or statistical characteristic to extract the embedded watermark. Watermark detection decides whether an image has been watermarked and if the watermark exists or not by calculating the correlation between the embedded watermark and the extracted one.

The goal of this paper is to propose a novel scheme for the copyright protection of colour images by using the visible watermark called COCOA. This visible watermarking algorithm is based on content and contrast aware (COCOA) with the Human Visible System (HVS) model to get the best trade-off between the embedding energy of the watermark and the perceptual translucence for a visible watermark. The rest of this paper is organized as follows. Related works about visible watermarking will be introduced briefly in Section 2. The details of the COCOA algorithm will be explained in Sections 3 and 4 will show the experimental results with discussion in Section 5, and the conclusion is in Section 6, respectively.

2. Related works

Digital contents embedded with visible watermarks will overlay recognizable but unobtrusive copyright patterns to identify its ownership. Therefore, a visible watermarking technique should remain details of the contents and ensure embedded patterns difficult or even impossible to be removed, and no one could use watermarked data illegally. An effective visible watermarking algorithm usually requires meeting a set of requirements [3,4]. These requirements include:

- The watermark in the marked digital contents should be obvious and recognizable to any person having normal or corrected visual accommodation, even if that person is color-blind. Clearly, the visible watermark should be visible in both color and monochrome images.
- It should be possible to adjust the strength of embedding applied to the digital contents by referring its characteristics of the digital contents, so that the watermark could be made as obtrusive or unobtrusive as desired without introducing any other artifacts. It should not only protect the digital contents from unauthorized uses but also prevent it from being so unattractive that no one is interested in viewing it.
- The patterns of the watermark in the embedded contents should be visible, and should form a recognizable symbol to identify content owners or providers.
- All details of the unmarked digital contents should be preserved in the marked digital ones. It means that corresponding pixel values in marked regions between the original and watermarked digital contents should be different in brightness, but the same in hue and saturation.

- The watermark should be very difficult to be removed or robust to attacks and this is the meaning of robustness. Therefore, watermark removal should be more expensive and labor intensive than purchasing the rights to use the digital data.

From the literature survey [5,6], the visible watermarking has captured greater attention than the invisible one [7] since there are not only different visible watermarking approaches either in spatial or transform domain, but also various visible watermark removal schemes. We now will briefly review the related works in visible watermarking and watermark removal techniques, respectively.

2.1. Visible watermarking

Visible watermarking techniques are used to protect the copyright of digital multimedia (audio, image or video) that have to be delivered for certain purposes, such as digital multimedia used in exhibition, digital library, advertisement or distant learning web, while illegal duplication is forbidden. Braudaway et al. [3] proposed one of the early approaches for visible watermarking by formulating the nonlinear equation to accomplish the luminance alteration in spatial domain. In this scheme, dimensions of the watermark image are equal to those of the host image. There is a one-to-one correspondence between pixel locations in the watermark image and those in the host image. According to their brightness, pixels in the watermark image can be divided into transparent and nontransparent categories. The brightness of each pixel in the host image in proportion to the nontransparent regions of the watermark will be increased or reduced to a perceptually equal amount by using a nonlinear equation while the brightness of each pixel in proportion to the transparent regions of the watermark will remain the same after watermark embedding. They formulate the nonlinear equation by using an approximately colour space, such as the CIE 1976 ($L^*u^*v^*$) space and the CIE ($L^*a^*b^*$) space, while various parameters of the nonlinear equation are applied to make the watermark difficult to be removed.

Meng and Chang [8] applied the stochastic approximation for Braudaway's method in the discrete cosine transform (DCT) domain by adding visible watermarks in the video sequences. Mohanty et al. [9] proposed a watermarking technique called dual watermarking which combines a visible watermark and an invisible watermark in the spatial domain. The visible watermark is adopted to establish the owner's right to the image and invisible watermark is utilized to check the intentional and unintentional tampering of the image. Chen [10] has proposed a visible watermarking mechanism to embed a gray level watermark into the host image based on a statistic approach. First, the host image is divided into equal blocks and the standard deviation in each block is calculated. The standard deviation value will determine the amount of gray value of the pixel in the watermark to be embedded into the corresponding host image.

Kankanhalli et al. [11] proposed a visible watermarking algorithm in the discrete cosine transform (DCT) domain. First, the host image and the watermark image are divided into 8×8 blocks. Next, they classify each block into one of eight classes depending on the sensitivity of the block to distortion and adopt the effect of luminance to make a final correction on the block scaling factors. The strength of the watermark is added in varying proportions depending on the class to which the image block belongs. Mohanty et al. [12] proposed a modification scheme on their watermark insertion technique of [9] in order to make the watermark more robust.

Hu and Kwong [13,14] implemented an adaptive visible watermarking in the wavelet domain by using the truncated Gaussian function to approximate the effect of luminance masking for the image fusion. Based on image features, they first classify the host and watermark image pixels into different perceptual classes. Then, they use the classification information to guide the pixel-wise watermark embedding. In high-pass subbands, they focus on image features, while in the low-pass subband, they use truncated Gaussian function to approximate the effect of luminance masking. Yong et al. [15] also proposed a translucent digital watermark in the DWT domain and used the error-correct code to improve the ability of anti-attacks.

Each of the above schemes wasn't devoted to better feature-based classification and the use of sophisticated visual masking models, so Huang and Tang [7] presented a contrast sensitive visible watermarking scheme with the assistance of HVS. They first compute the CSF mask of the discrete wavelet transform domain. Secondly, they use a square function to determine the mask weights for each subband. Thirdly, they adjust the scaling and embedding factors based on the block classification with the texture sensitivity of the HVS. However, their scheme should further consider the following issues:

1. The basis function of the wavelet transform plays an important role during the application of CSF for the HVS in the wavelet transform domain, but the study [7] didn't consider this key factor.
2. The embedding factors emphasize too much weight on the low frequency domain, rather than equal emphasis on the medium-to-high frequency domains.
3. The interrelationship of block classification and the characteristics of the embedding location should be further analyzed.

For the first issue, the direct application of CSF for the HVS in the wavelet transform domain needs to be further studied [16–20] while the basis function of the wavelet transformation is a critical factor affecting the visibility of the noise in the DWT domain. For the second issue, the watermark embedding in the low frequency components results in high degradation of the image fidelity. How to get the best trade-off between the visibility of the watermark and the capability of resistance for removal still needs to be further justified. For the third issue, the plane, edge and texture block classification in the study [7] is a genuine approach. However, the local and global characteristics of wavelet coefficients should be carefully considered, and the content adaptive approach is necessary for making the optimal decision.

2.2. Watermark removal and image recovery

Since the visible watermark is embedded within the images, it is not unusual that attackers would try any means to remove the watermark so that they can use the images freely without any copyright concerns. If the contour of an embedded visible watermark is completely removed or greatly distorted without introducing serious visual quality degradation, it would be difficult for the content owner to claim the infringement by the illegal users. Even in this existing situation, a good visible watermark scheme becomes the barrier for the attackers since expensive human labours would be needed in order to remove the watermark itself.

Regarding the removal technique, the image recovery method [21] can remove visible watermarking patterns consisting of thin lines, and a few human interventions of image-inpainting approach of [22] can deal with the patterns of thick lines. However, the iterative process of image-inpainting in [22] is costly and time-consuming. Pei and Zeng [23] proposed another image recovery algorithm for removing visible watermarks which is simple, fast, and with less human intervention. The method mainly utilizes independent component analysis (ICA), i.e. joint approximate diagonalization of eigenmatrices (JADE), second-order blind identifica-

tion (SOBI), and FastICA to separate host images from watermarked and reference images. The algorithm includes three phases: watermarked area segmentation, reference image generation, and image recovery. In their experiments, five different visible watermarking methods [3,8,10,12,13] and three public domain images [23] are tested. The experimental results show that their algorithm can successfully remove the visible watermarks, and the algorithm itself is independent of both the adopted ICA approach and the visible watermarking method. Interested readers can refer to [23] for detailed information.

In this study, we will also examine COCOA's robustness by checking whether the proposed algorithm can resist the watermark removal and image recovery attacks.

3. The COCOA visible watermarking algorithm

In general, a useful visible watermarking technique must meet the following requirements according to [7,22]: the perceptibility of host image details, the visibility of watermark patterns in embedded contents and robustness. To be more specific, contents should not be rendered useless after being visibly watermarked, and all the details in the original image should remain visible. In addition, visible watermarks often consist of meaningful pattern, symbols, trademarks, or logos to identify content providers or owners, and these copyright data should be easily recognized from the watermarked images. On the other hand, embedded visible watermark patterns should be difficult or impossible to be removed unless exhaustive and costly user interventions are adopted. Therefore, the robustness is a critical issue for visible watermarking which is generally not widely discussed in previous studies like [3,5,7–14,24]. To address this issue, the proposed COCOA algorithm has put great emphasis on the design to enhance its robustness.

Nevertheless, in this proposed method, the robustness and translucence of COCOA are in confliction with each other. If we increase the energy of watermark to improve its robustness, the problem we get is perceptual translucence decreasing with less image fidelity and vice versa. Therefore, we have to decrease the energy of the watermark to get good perceptual translucence, while the embedded watermark will still be robust to intentional or unintentional signal processing attacks. In addition, HVS (Human Visual System) is the key factor we have found in providing the good translucence of the watermarked image and a better robustness [3,24]. Human Visual System research offers the mathematical models on how humans see the world, and a lot of works have been devoted to understanding HVS [16–18,20]. Psychovisual studies have shown that human vision has different sensitivity from various spatial frequencies (frequency subbands). Common HVS models are composed of image dependent or independent Just Noticeable Difference (JND) thresholds, so the HVS by using the contrast sensitive function (CSF) and noise visibility function (NVF) is collaborated in this study and will be explained in brief as follows.

3.1. CSF (contrast sensitive function)

For watermarked images, there has been a need for good metrics for image quality that incorporates properties of the HVS. The visibility thresholds of visual signals are studied by psychovisual measurements to determine the thresholds. These measurements were performed on sinusoidal gratings with various spatial frequencies and orientations by the given viewing conditions. The purpose of such study was to determine the contrast thresholds of gratings by the given frequency and orientation. Contrast as a measure of relative variation of luminance for periodic pattern such as a sinusoidal grating is here given by the equation:

$$C = (L_{\max} - L_{\min})/(L_{\max} + L_{\min}) \tag{1}$$

where $L_{\max}$ and $L_{\min}$ represent maximal and minimal luminance of a grating. Reciprocal values of contrast thresholds express the contrast sensitivity (CS), while Mannos and Sakrison [16] originally presented a model of the contrast sensitive function (CSF) for luminance (or grayscale) images is given as follows:

$$\mathrm{CSF}(f) = 2.6 * (0.0192 + 0.114 * f) * e^{-(0.114*f)^{1.1}} \tag{2}$$

where $f = \sqrt{f_x^2 + f_y^2}$ is the spatial frequency in cycles/degree of visual angle (f_x and f_y are the spatial frequencies in the horizontal and vertical directions, respectively). Fig. 2(a) depicts the CSF curve which characterizes luminance sensitivity of the HVS as a function of normalized spatial frequency. According to the CSF curve, we can see that the HVS is most sensitive to normalized spatial frequencies

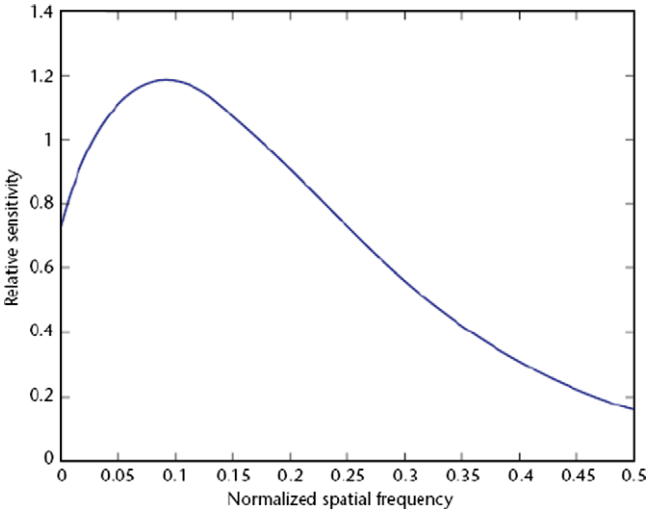

(a)

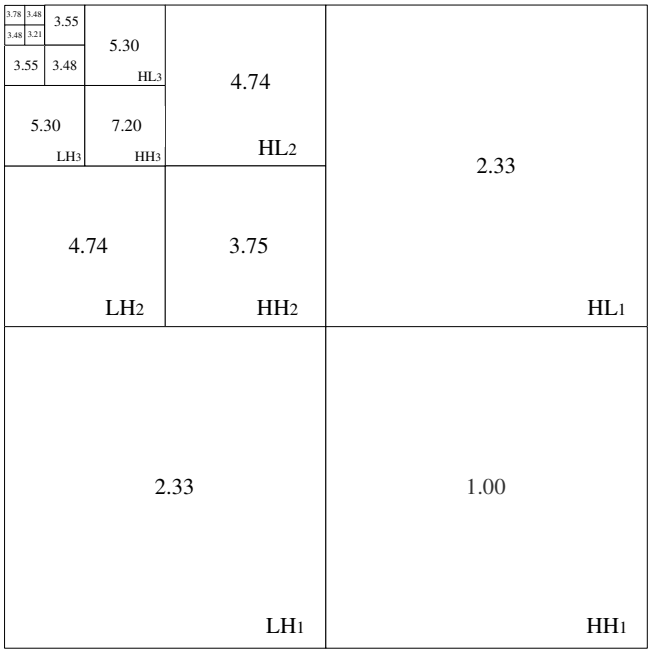

(b)

Fig. 2. (a) Luminance of contrast sensitive function. (b) DWT CSF mask with 11 unique weights after 5-level wavelet pyramidal decomposition.

between 0.025 and 0.125 and less sensitive to low and high frequencies [3]. Therefore, the sensitivity falls off as the frequency values drifts on low and high frequency sides. Under such circumstance, this knowledge from CSF can be used to develop a simple image independent HVS model.

CSF masking [17,18] is one way to apply the CSF in the discrete wavelet domain. CSF masking refers to the method of weighting the wavelet coefficients relative to their perceptual importance. In [18], the DWT CSF mask utilizes the information in all of the approximation subbands as well as all of the detail subbtands to yield 11 unique weights in the mask. All of the weights are normalized so that the lowest weight is equal to one. The 11 weights of DWT CSF mask are shown in Fig. 2(b) after 5-level wavelet pyramidal decomposition. From the weight values of Fig. 2(b), the HVS is most sensitive to the distortion in mid-frequency regions (level 3), and sensitivity falls off as the frequency value drifts on both sides (level 1, 2, 4 and 5). To adopt the watermark intensity to both global and local characteristics of the source images, the DWT coefficients of the host image will be modified according to the following equation:

$$Y^{\lambda}_{i,j,\theta} = \alpha_{\lambda,\theta} \times X^{\lambda}_{i,j,\theta} + \beta_{\lambda,\theta} \times S^{\lambda}_{i,j,\theta} \tag{3}$$

where λ(=1, 2, 3, 4, 5) denotes the decomposition level, (i, j) indicates the spatial location, θ(=1, 2, 3, 4) is the orientation, X and S are the decomposed wavelet coefficients of the original image and the watermark, respectively, Y is the composite watermarked DWT coefficient. The scaling factor $\alpha_{\lambda,\theta}$ and the modulation rate $\beta_{\lambda,\theta}$ are found using the mathematical model developed by exploiting perceptual weighting masks derived from the luminance CSF, and the sensitivity of the HVS to ensure the perceptual quality of the image in this way is better preserved. In Eq. (3), the adequate scaling factor $\alpha_{\lambda,\theta}$ and the modulation rate $\beta_{\lambda,\theta}$ are found using square function [7,13] to approximate the effect of CSF masking since the maximum weight is 7.20 from Fig. 2(b). The scaling factors of $\alpha_{\lambda,\theta}$ are decreased as the frequency values of the wavelet coefficients drift away from the mid frequency level, and that of $\beta_{\lambda,\theta}$ is increased. $\alpha_{\lambda,\theta}$ and $\beta_{\lambda,\theta}$ are described as:

$$\begin{aligned} \alpha_{\lambda,\theta} &= 1 - \frac{(7.20 - r_{\lambda,\theta})^2}{7.20^2} \\ \beta_{\lambda,\theta} &= 0.01 + \frac{(7.20 - r_{\lambda,\theta})^2}{7.20^2} \end{aligned} \tag{4}$$

where $r_{\lambda,\theta}$ represents the wavelet coefficient CSF of the perceptual importance weight for each subband at different decomposition level. The values of $\alpha_{\lambda,\theta}$ and $\beta_{\lambda,\theta}$ are restricted within certain range to avoid the abrupt change of DWT coefficients. If NVF and detection thresholds for DWT coefficients have also been considered during the implementation, the final formulas of COCOA in this study will be further revised in Eq. (9) and Eq. (10).

3.2. NVF (noise visibility function)

Many schemes embedded the watermark as random noise in the whole host image with the same strength regardless of the local properties of the host image, so the visible artifacts are easily noticed in the flat regions. Voloshynovskiy et al. [19] presented a stochastic approach based on the computation of a NVF (noise visibility function) that characterizes the local image properties and identifies texture and edge regions. Accordingly, when the local variance is small, the image is flat, and a large enough variance indicates the presence of edges or highly texture areas. Because human eyes are more sensitive to changes in the flat regions than in the edge regions of the image, watermarking techniques can increase the energy of watermark in the edges and high textured areas of the image, and reduce it in smooth regions in similar peak signal-to-noise ratio (PSNR). This allows us to determine the optimal locations and the strength of the watermark during the watermark embedding stage. Therefore, this concept from NVF can be used to develop a simple image dependent HVS model.

They developed three such NVF functions as follows:

3.2.1. NVF function with non-stationary Gaussian model

$$\mathrm{NVF}(i,j) = \frac{1}{1+\sigma_x^2(i,j)} \tag{5}$$

with

$$\sigma_x^2(i,j) = \frac{1}{(2L+1)^2} \sum_{k=-L}^{L} \sum_{l=-L}^{L} (x(i+k,j+l) - \bar{x}(i,j))^2$$

$$\bar{x}(i,j) = \frac{1}{(2L+1)^2} \sum_{k=-L}^{L} \sum_{l=-L}^{L} x(i+k,j+l)$$

where L represents width of window, $\sigma_x^2(i,j)$ denotes the local variance in a window centered on the wavelet coefficient with coordinates (i, j). Therefore, the NVF is inversely proportional to the local image properties defined by the local variance.

3.2.2. NVF function with stationary GG (generalized Gaussian) model

$$\mathrm{NVF}(i,j) = \frac{w(i,j)}{w(i,j)+\sigma_x^2} \tag{6}$$

where $w(i,j) = \gamma[\eta(\gamma)]^{\gamma}/\|\rho(i,j)\|^{2-\gamma}$ and σ_x^2 represent the global variance of host image. $\eta(\gamma) = \sqrt{\Gamma(3/\gamma)/\Gamma(1/\gamma)}, \Gamma(t) = \int_0^{\infty} e^{-u}u^{t-1}du$ (gamma function) and $\rho(i,j) = (x(i,j) - \bar{x}(i,j))/\sigma_x$. γ is the shape parameter, and $\rho(i,j)$ is determined by the local mean and the local variance. For most of real images, the shape parameter is in the range $0.3 \leqslant \gamma \leqslant 1$.

3.2.3. NVF function with empirical model

$$\mathrm{NVF}(i,j) = \frac{1}{1+\tau\sigma_x^2(i,j)} \tag{7}$$

where $\tau = D/\sigma_{x\max}^2$ is a tuning parameter, and $\sigma_x^2(i,j)$ is the local variance. $\sigma_{x\max}^2$ is the maximum local variance and $D \in [50, 100]$ is an experimentally determined parameter.

NVF characterizes the local image properties and identifies the texture and edge regions. It takes the values between zero and one. Higher values of NVF indicate flat region, and vice versa: lower values of NVF indicate textured or edge region. Since human eyes are less sensitive in texture and edge regions, so we can embed the watermark strongly. On the other hand, the smooth regions should be least modified to avoid significant image distortion. Incidentally, the quality of the watermarked image is least degraded. From the visual quality comparison in [19], the adaptive scheme based on NVF calculated from stationary GG model is superior to other schemes. In this study, different models are also tested, and as a result, we agree with the findings in [19] where the adaptive stationary GG model outperforms other models.

In [19], the authors suggested an embedding equation for invisible watermarking: $Y_{i,j} = X_{i,j} + (1 - \mathrm{NVF}_{i,j}) \times \beta_1 \times S_{i,j} + \mathrm{NVF}_{i,j} \times \beta_2 \times S_{i,j}$ where $\beta_1$and β_2 denote the watermark strength in busy and flat image regions. However, we have found such format not adequate for visible watermark embedding, since the weighting of visible watermark is generally larger than invisible watermarking. Without further modification, direct implementation will result in an overflow situation with obvious image degradation. Through these empirical studies, the final COCOA embedding equation will be given in Eq. (10).

3.3. Detection thresholds for DWT coefficients

In order to further improve the HVS model for better image quality, the knowledge on the detection thresholds for DWT coefficients should also be obtained. Watson et al. [20] proposed a mathematical model for DWT noise detection thresholds where visibility Y is a function of level, orientation, and visual display resolution for 9/7 biorthogonal wavelets [25]. The model is given by

$$\log Y_{\lambda,\theta} = \log a + k(\log f_\lambda - \log g_\theta f_0)^2 \tag{8}$$

where a is the minimum threshold occurring at spatial frequency $g_\theta f_0$, f_λ is the spatial frequency of decomposition level λ, and g_θ shifts the minimum by an amount that is a function of orientation. For thresholds of visibility, the quantization matrices are constructed by using a quantization factor for each level and orientation that will result in a quantization error which is just at the threshold of visibility. For the uniform quantization and a given quantization factor Q, the largest possible coefficient error is $Q/2$. The amplitude of the resulting noise is approximately $A_{\lambda,\theta}\cdot Q/2$ given $A_{\lambda,\theta}$ being the basis function amplitudes. Table 1 shows the basis function amplitudes for a 5-level 9/7 DWT. These visibility thresholds express the frequency sensitivity of HVS in DWT domain, while the basis function amplitude $A_{\lambda,\theta}$ at different wavelet level and orientation should be considered for watermark embedding. Therefore, COCOA integrates these factors into the design of modulation rate $\beta_{\lambda,\theta}$ in Eq. (9).

As shown in the above discussion, we found that the direct application of CSF square function in [7] emphasizes too much weight in the low DWT frequency domain after implementing the CSF based visible watermarking [7]. Therefore, the CSF only based watermarking approach generally results in the watermarked images with PSNR values below 30 dB for many common used 512×512 colour images. This finding is consistent with the PSNR data in [7] since their watermarked Lena image has only 27.6421 dB PSNR value. Even when PSNR values do not truly represent the visual quality for the visible watermark images, the values still have a positive correlation with the image fidelity and consequently become widely adopted in many research articles. Due to its popularity, this metric therefore can be used as the reference/baseline index. Higher PSNRs do have a closer image similarity with the host images, and among the purposes of this study, improving the PSNR values with a better robustness against attacks is certainly an important issue.

In addition, there are not enough high frequency components of the watermarked image to resist the common image signal processing like compression attacks which will be examined in next section. According to this observation, the concept of DWT noise detection threshold of [20] is adopted here to fine tune the perceptual weights by the basis function amplitudes $A_{\lambda,\theta}$, while the CSF masking for 9/7 filter becomes integrated for the proposed algorithm. Therefore, the perceptual weighting is modified according to this research as follows:

$$\begin{cases} \beta_{\lambda,\theta} = \left[\frac{0.4+(7.20-r^\lambda)^2}{7.20^2}\right] \times A_{\lambda,\theta} \\ \text{if} \quad \beta_{\lambda,\theta} \geq 0.2,\ \beta_{\lambda,\theta} = 0.2 \\ \alpha_{\lambda,\theta} = 1 - \beta_{\lambda,\theta} \end{cases} \tag{9}$$

Table 1
Basis function amplitudes for a 5-level 9/7 DWT [20].

Orientation	Level				
	1	2	3	4	5
LL	0.62171	0.34537	0.18004	0.09140	0.045943
HL	0.67234	0.41317	0.22726	0.11792	0.059758
LH	0.67234	0.41317	0.22726	0.11792	0.059758
HH	0.72709	0.49428	0.28688	0.15214	0.077727

Here, $\alpha_{\lambda,\theta}$ and $\beta_{\lambda,\theta}$ are scaling and embedding factors; λ represents the DWT level, θ is the orientation and r^λ is the wavelet coefficient CSF of the perceptual importance weight as shown in Fig. 2(b). Meanwhile, $\alpha_{\lambda,\theta}$ and $\beta_{\lambda,\theta}$ are the global characteristics of the host image, and they are independent to the digital images. To avoid the abrupt change of DWT coefficients, the values of $\alpha_{\lambda,\theta}$ and $\beta_{\lambda,\theta}$ are restricted within the range of [0.8, 1] and [0, 0.2], respectively.

In order to further improve the application of block classification by simply categorizing three type blocks in [7], the local and global characteristics in the DWT domain is considered. In our COCOA scheme, a stochastic image model for watermark embedding is adopted by using the NVF which characterizes the local image properties and identifies texture and edge regions. In our scheme, we have found that the stationary GG model is the most appropriate approximation among others in the embedding stage, and the estimated shape parameter for $\gamma = 0.65$, and width of the window is three. In addition, the Watson's quantization matrix [20] is adopted in the viewing process to get the best quality of the watermarked image. Therefore, the COCOA embedding relationship is concluded as follows:

$$Y^\lambda_{i,j,\theta} = \alpha_{\lambda,\theta} \times X^\lambda_{i,j,\theta} + (1 - \mathrm{NVF}_{i,j}) \times \beta_{\lambda,\theta} \times S^\lambda_{i,j,\theta} + \mathrm{NVF}_{i,j} \times K \times S^\lambda_{i,j,\theta} \tag{10}$$

where (i, j) indicates the spatial location, X and S are the decomposed wavelet coefficients of the original image and the watermark, respectively, $\mathrm{NVF}_{i,j}$ is defined in Eq. (6) and the relationship of $\alpha_{\lambda,\theta}$ and $\beta_{\lambda,\theta}$ is defined Eq. (9). The constant K denotes the embedding watermark strength for flat regions, and the empirical value 0.08 is adopted for this algorithm which gives the best experimental performance while watermarked images are at values >30 dB.

In summary, the complete design of the proposed algorithm is summarized in the following guidelines and the flow chart is shown in Fig. 3:

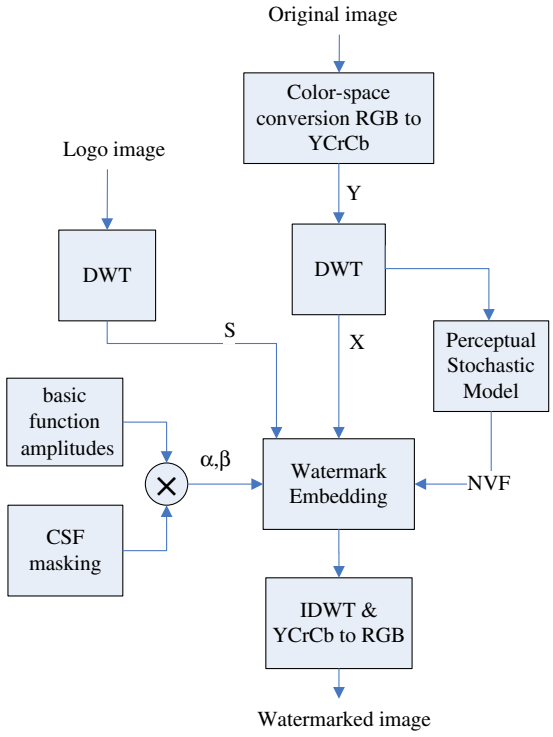

Fig. 3. The flow chart of the proposed COCOA visible watermarking approach.

3.3.1. The COCOA watermarking embedding algorithm

(1) The host colour image is converted in the colour space domain from RGB to YCrCb.
(2) By using 9/7 biorthogonal filter from [25], compute the wavelet coefficients of Y component from the host colour image and grayscale watermark image, respectively. If the width or height of the watermark is not the same as the one of the host image, it could be proportionally scaled to the host image.
(3) Modify the DWT coefficients of the host image by using the following equation for each spatial location (i, j), where λ(=1, 2, 3, 4, 5) denotes the decomposition level and θ(=1, 2, 3, 4) is the orientation.

$$Y^{\lambda}_{i,j,\theta} = \alpha_{\lambda,\theta} \times X^{\lambda}_{i,j,\theta} + (1 - \mathrm{NVF}_{i,j}) \times \beta_{\lambda,\theta} \times S^{\lambda}_{i,j,\theta} + \mathrm{NVF}_{i,j} \times K \times S^{\lambda}_{i,j,\theta}$$

Note: X and S are the decomposed wavelet coefficients of the original image and the watermark, respectively. $\mathrm{NVF}_{i,j}$ is defined in Eq. (6), and the relationship of $\alpha_{\lambda,\theta}$ and $\beta_{\lambda,\theta}$ is defined in Eq. (9). The constant K value is 0.08.

(4) Inverse transform the DWT coefficients of the host image to obtain a watermarked image.

Note: The current COCOA algorithm implementation specifically applies the 9/7 biorthogonal DWT filter since the DWT CSF mask with 11 unique weights from Fig. 2(b) and the basis function amplitudes in Table 1 are all obtained by using the 9/7 filter. The DWT CSF mask weight, basis function amplitudes and the constant K of Eq. (10) need to be recalculated if different filter is being used in order to fine tune the best quality of perceptual translucence and noise reduction for COCOA watermarking algorithm.

4. Experiments

The proposed COCOA visible watermarking algorithm has been implemented and intensively tested by using the commonly available colour images from the USC image database [26]. Two grayscale watermarks of logo image adopted in the experiments are shown in Fig. 4: 4(a) NCTU logo (school logo) and 4(b) IIM logo (department logo). Since the CSF based visible watermark technique from [7] has shown better performance than the methods from [14] and the AiS Watermark Pictures Protector [27], we compared the results gained by [7] with the proposed approach and the those of performances of the 512×512 colour Lena, F16 and Baboon images which are tabulated for demonstration purpose in Table 2 and Figs. 5–9.

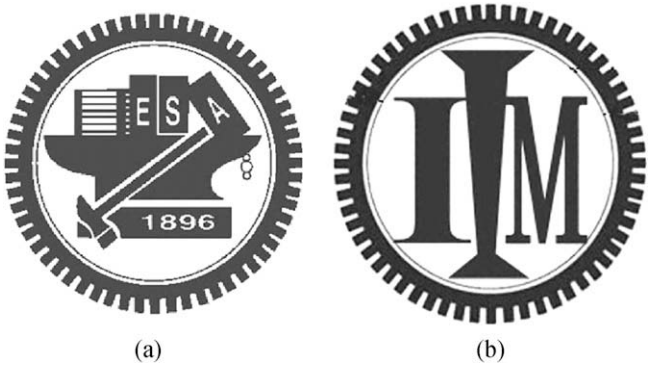

Fig. 4. Two watermark images (a) NCTU logo and (b) IIM logo.

Table 2
PSNR summary of COCOA watermarked color images.

Image	Watermark	PSNR value	
		Method [7]	COCOA method
Lena	NCTU	27.0 dB	31.6 dB
Baboon	NCTU	27.1 dB	30.2 dB
F16	NCTU	28.8 dB	31.6 dB
Lena	IIM	26.8 dB	32.7 dB
Baboon	IIM	27.2 dB	31.0 dB
F16	IIM	28.1 dB	32.4 dB

The detailed analyses are categorized as follows:

4.1. PSNR (peak signal-to-noise ratios)

To make a fair comparison with the method from [7], it is better to embed the same watermark for the same cover image. However, the watermark used in [7] is not available and we then embed two logo watermarks from Fig. 4 to enable the best possible performance comparison. The tabulated results from Table 2 disclose that our COCOA watermarking scheme can bring better statistical results and achieve higher PSNR values (above 30 dB) than the method in [7] where the PSNRs are generally below 30 dB. If the image is with PSNR less than 30 dB, we can assume that its watermark embedded more strongly than the one with PSNR higher than 30 dB. Since the values of α^k and β^k are restricted within the range of [0.9, 1] and [0.01, 0.1], respectively, in [7] to avoid the abrupt change of DWT coefficients, heavy weight of α^k results the watermarked image of [7] can not achieve PSNR >30 dB. On the other hand, the scaling factor $\alpha_{\lambda,\theta}$ and modulation rate $\beta_{\lambda,\theta}$ of COCOA have a wider dynamic range which can be adjusted for higher PSNR values. The low PSNRs have a positive correlation with the degradation in image quality and this denotes that the fidelity of images from our method is better than the method solely based on CSF.

4.2. Visual quality comparison

In Figs. 5–9, for each sample of Lena, Baboon and F16, we demonstrate three images: the original image, watermarked image resulted from [7], the proposed COCOA approach. The logo image applied in Fig. 5 is from Fig. 4(a) and the logo image applied in Fig. 6 is from Fig. 4(b). A comparison of the photo pairs between Fig. 5(b,c), (e,f), and (h,i) shows clearly that the COCOA method obtains the closest luminance maintenance as compared with the original ones. The watermarked images using [7] have a more blurry effect in the contour than that of the COCOA method, and similar observation is also obtained from the pairs of Fig. 6(b,c), (e,f) and (h,i).

To further compare the details in the watermarked images, Figs. 7–9 demonstrate some of the close-ups for comparison: Fig. 7(a)–(f) are the close-ups of Lena image from Figs. 5 and 6; Fig. 8(a)–(f) are the close-ups of Baboon image from Figs. 5 and 6; Fig. 9(a)–(f) are the close-ups of F16 image from Figs. 5 and 6. It is very clear that the edges and thin lines of the watermark are blurred in Figs. 7–9(b) and (e). However, by observing the close-ups from Figs. 7 and 9(c) and (f), we see that the watermark patterns are still with sharp edges, and the logo watermark is evidently embedded. For the text pattern, the text of character *A* in Figs. 7 and 8(c) is with sharper edge than the same character in Figs. 7 and 8(b). The outlines in Figs. 7–9(c) are much clearer than those in Figs. 7–9(b). These experiments indicate that our visible COCOA watermarking scheme corresponds to higher PSNRs with a better image quality than the approach of [7].

4.3. Median filtering

The robustness of the COCOA visible watermark technique should be examined for comparison. The attacks in StirMark [28]

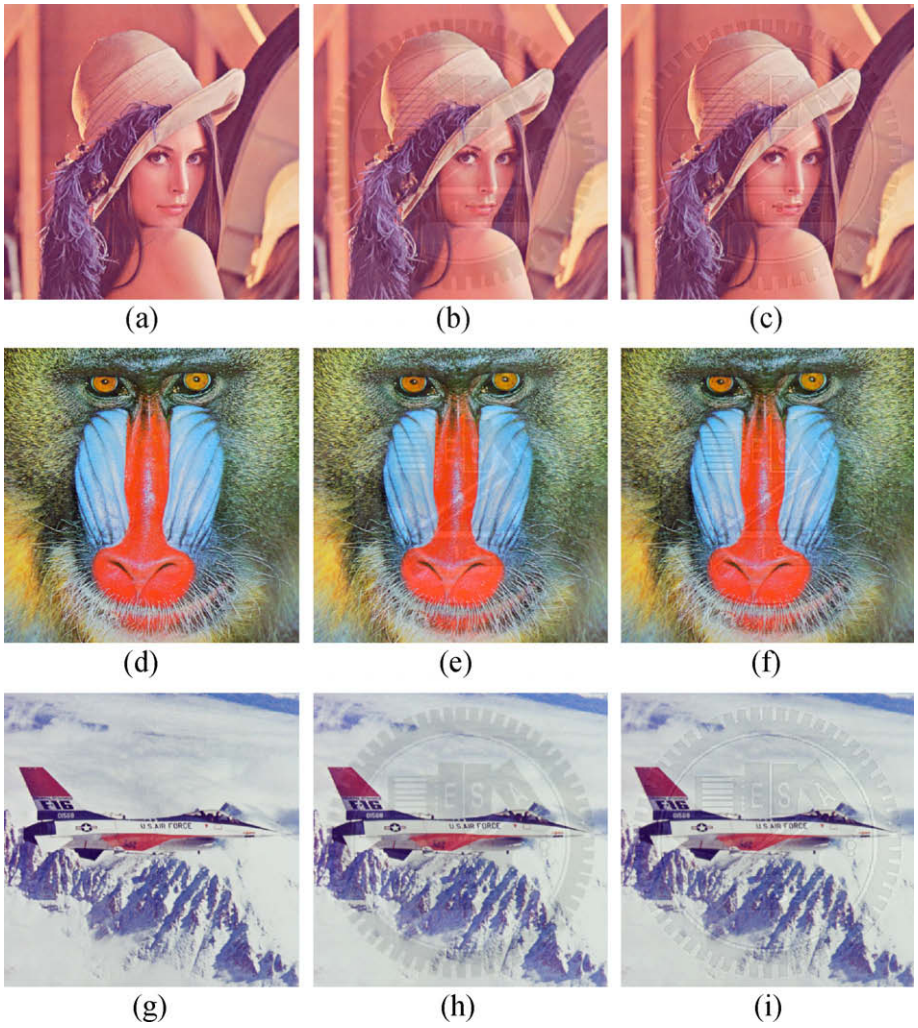

Fig. 5. The visual quality comparison of original and watermarked images by embedding logo of Fig. 4(a). (a), (d) and (g) are original Lena, Baboon, F16 images. (b), (e) and (h) are watermarked images by the method [7]. (c), (f) and (i) are watermarked images by COCOA algorithm.

have been thoroughly tested and we have found that the visual difference in Median filtering and compression is more significant than others. Therefore, the Median filtering and compression performance is demonstrated for the purpose of illustration. Median filtering from StirMark [28] software is adopted here for this attack. Since the results of 3×3 and 5×5 median filtering are similar to the illustrations shown in Figs. 7–9, a stronger attack as 7×7 median filtering is applied here for the purpose of demonstration. The PSNR values before and after the median filtering are tabulated in Table 3.

There are two columns of PSNR values for both methods labelled "after". The pure "after" column means those PSNR values are gained after comparison between the filtered watermarked images and the original images. The after(wm) column means those PSNR values are the results of comparison between the filtered watermarked images and the watermarked images. From Table 3, we can find that the PSNR values (after(wm) column) are almost the same for both methods when the filtered watermarked images are compared with the watermarked images. However, the PSNR values (after column) are higher when the filtered watermarked images are compared with the original images by the COCOA approach than by the method of [7]. Therefore, this statistic indicates that the image quality of watermarked images before and after filtering is higher by the COCOA approach than by the method of [7]. To further investigate the effect of the median filtering, the visual difference can be illustrated by the close-up comparison. Fig. 10(a), (d) and (g) are the close-ups from Figs. 5 and 6 showing the original Lena, Baboon and F16 images, respectively. Fig. 10(b), (e) and (h) are the close-ups of watermarked image by the method of [7] after 7×7 median filtering. Fig. 10(c), (f), and (i) are the close-ups of watermarked image by the COCOA method after 7×7 median filtering. By comparing Fig. 10(a)–(c), the median filtered images became blurry, but Fig. 10(c) has a sharper contour of the watermark than that of Fig. 10(b). It is apparent that the logo pattern (i.e. the characters of E, S, A) is still detectable in Fig. 10(f), but is blurred and hard to recognize in Fig. 10(e). In addition, the stripes of logo pattern on the left side of close-up of Fig. 10(e) are also less evident than those on the Fig. 10(f).

The texts in Fig. 10(h) and (i) have been unrecognizable after the median filtering (for example, number 01568 on the plane tail is too fuzzy to be identified in Fig. 10(h) and (i)) but the watermark of Fig. 10(i) still has closer outlines than Fig. 10(h). Therefore, the COCOA technique outperforms [7] by using the median filtering attack, and as we see from the above observation, the visibility of watermark is higher by COCOA approach.

4.4. JPEG2000 compression

The robustness of the compression attack is also tested here and JPEG2000 [29] is adopted as the compression tool. The PSNR values

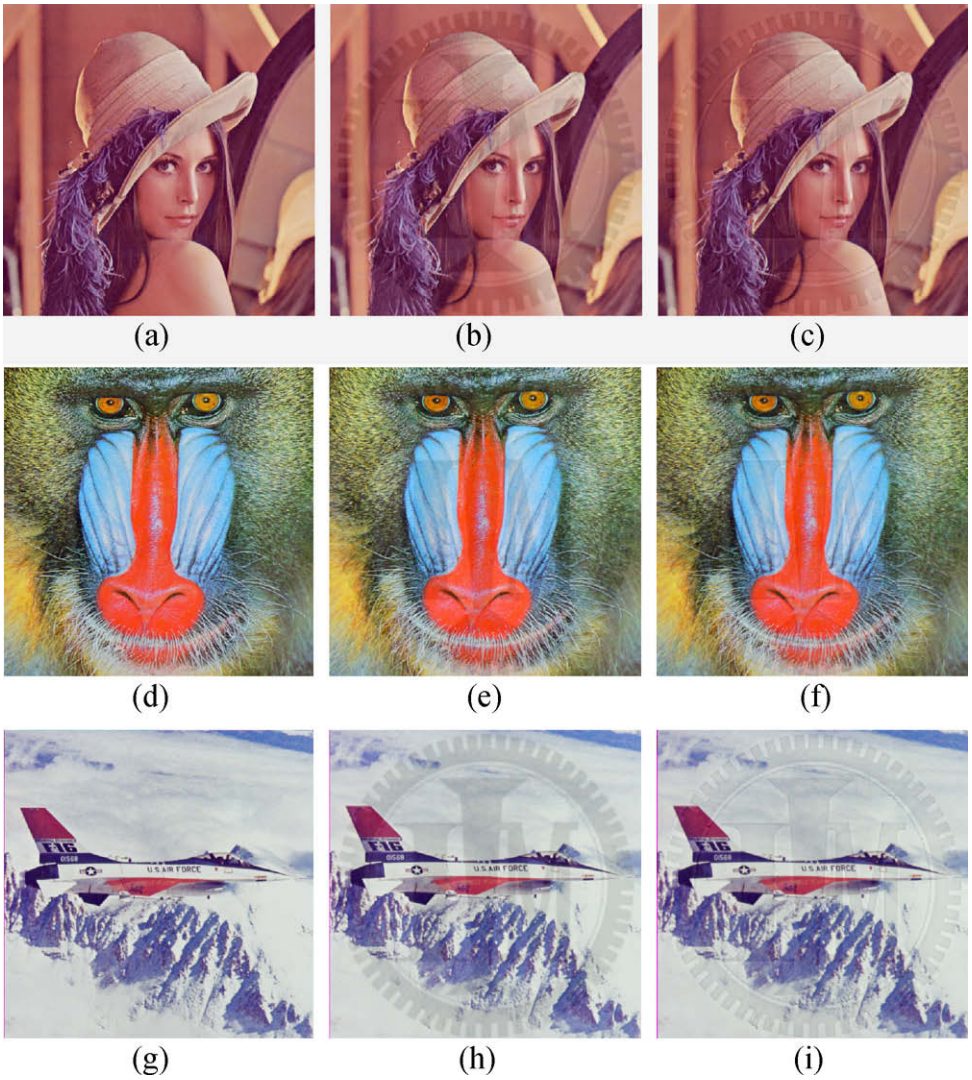

Fig. 6. The visual quality comparison of original and watermarked images by embedding logo of Fig. 4(b). (a), (d) and (g) are original Lena, Baboon, F16 images. (b), (e) and (h) are watermarked images by the method of [7]. (c), (f) and (i) are watermarked images by COCOA algorithm.

before and after the JPEG2000 compression are tabulated in Table 4. The compression ratio is set at a reasonable ratio of 100:3 between the uncompressed image and the compressed image. There are two columns of PSNR values for both methods labelled "after" and their meanings are the same as mentioned in the section on median filtering attack. From Table 4, we find that the PSNR values (after(wm) column) are almost the same for both methods when the compressed watermarked images are compared with the watermarked images. However, the PSNR values (after column) are higher when the compressed watermarked images are compared with the original images by the COCOA approach than by the method of [7]. Therefore, this statistic indicates that the image quality of watermarked images before and after compression is higher by the COCOA approach than by the method of [7].

To further investigate the effect of compression, the visual difference can be illustrated by a close-up comparison. Fig. 11(a), (d), and (g) are the close-ups from Figs. 5 and 6 showing the original Lena, Baboon and F16 images, respectively. Fig. 11 (e) and (h) are the close-ups of watermarked image by the method of [7] after JPEG2000 compression. Fig. 11(c), (f) and (i) are the close-ups of watermarked image by the COCOA method after JPEG2000 compression. By comparing Fig. 11(a)–(i), the compressed images maintain the details of the logo pattern, but the character of A is more apparent in Fig. 11(c), (f) and (i) than in Figs. 11(b), (e) and (h). In addition, the stripes of the logo pattern are almost disappearing in Fig. 11(e) while still detectable in Fig. 11(f). This observation is consistent with the claim of our discussion in Section 2, that the embedding factors in [7] emphasize more weights in the low frequency domain, rather than in the medium-to-high frequency domain where images with less high frequency watermark signals will easily suffer during the compression attack. Therefore, the proposed technique outperforms [7] by using JPEG2000 compression attack and as we see from the above comparison, the visibility of watermark is surely higher by this proposed approach.

4.5. Image recovery and watermark removal attack

To examine COCOA's robustness for watermark removal attacks, we have implemented the method of [22,23] for comparison. By applying the method of [23] to the watermarked images with campus logo by the methods of [3,7,8,12,13,10], the watermark can be clearly removed in our simulation. However, Figs. 12–14 illustrate the results of the image recovery attack from [23] on the COCOA watermarking approach where the logo patterns slightly disappear but still exist and the contours are recognizable in Figs. 12–14(b) and (d). The results are confirmed by Dr. Zeng of [23] for the simulation works.

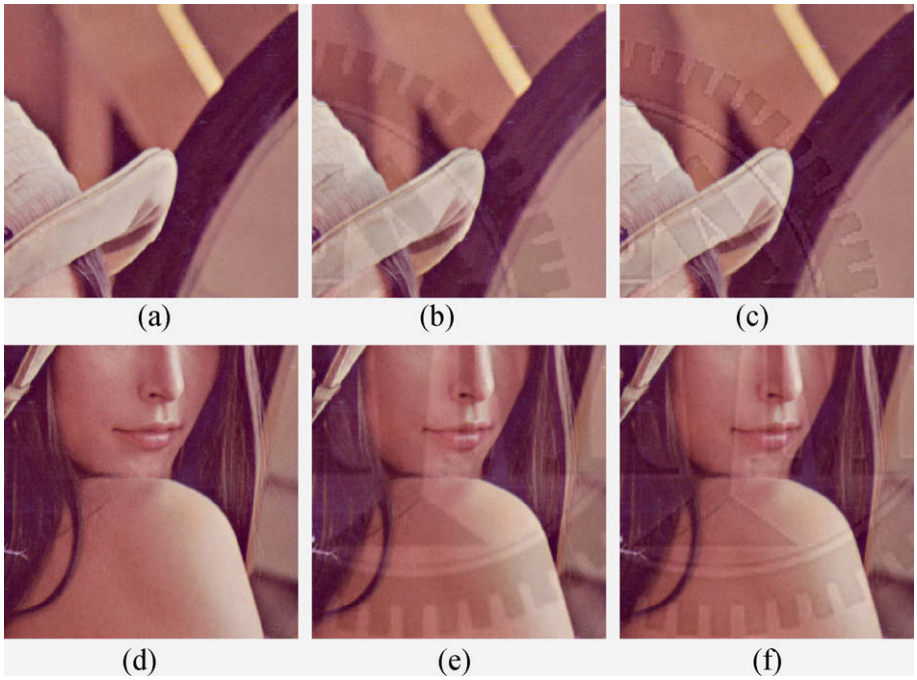

Fig. 7. The visual quality comparison of close-ups for Lena image. (a) and (d) are part of the original Lena image. (b) and (e) are watermarked Lena images by the method [7]. (c) and (f) are watermarked Lena images by COCOA algorithm.

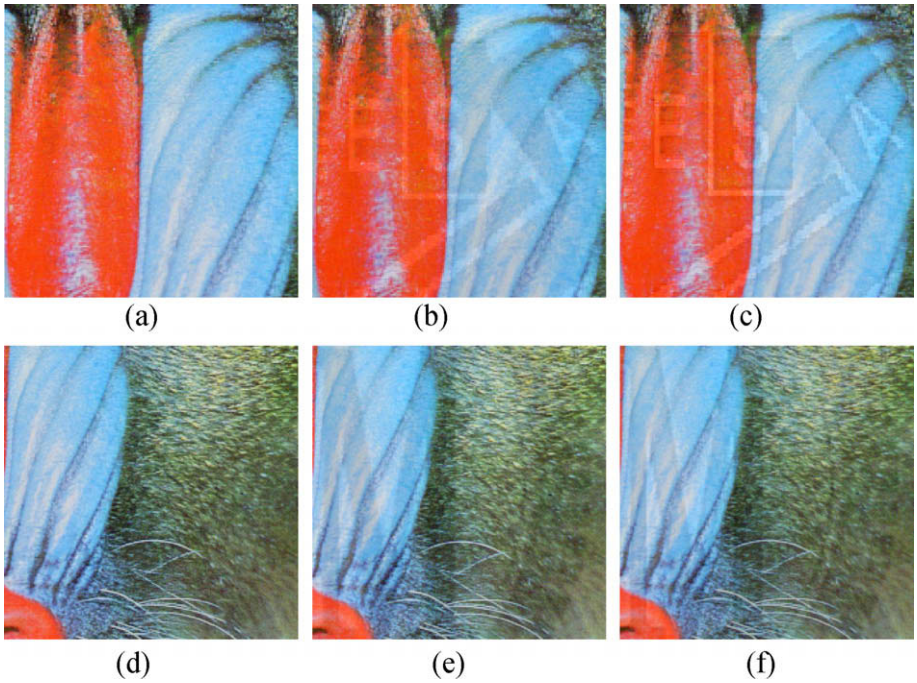

Fig. 8. The visual quality comparison of close-ups for Baboon image. (a) and (d) are part of the original Baboon image. (b) and (e) are watermarked Baboon images by the method [7]. (c) and (f) are watermarked Baboon images by COCOA algorithm.

Since the watermark removal scheme in [23] can remove the watermark by the methods of [3,7,8,12,13,10] but the COCOA approach can resist such an attack, we can conclude that the COCOA visible scheme certainly outperforms those methods with the robustness comparison.

In addition, the image-inpainting based watermark removal technique [22] is also simulated for the COCOA watermarked images of Boat and Peppers. Fig. 15(b) and (d) demonstrate that the COCOA watermarked images can resist this kind of attacks, since the visible watermark is still visible after the process.

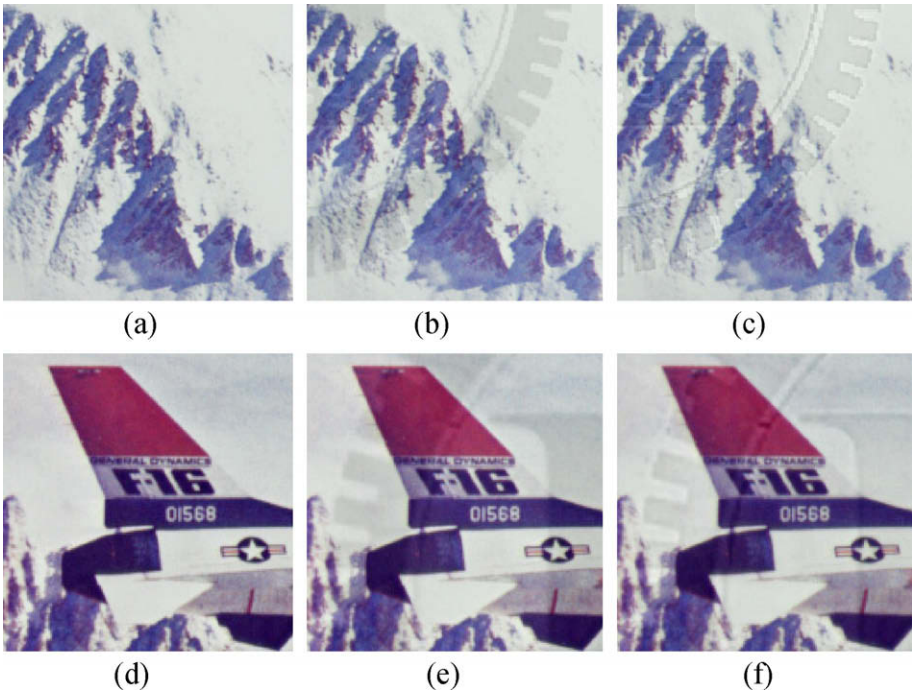

Fig. 9. The visual quality comparison of close-ups for the F16 image. (a) and (d) are part of the original F16 image. (b) and (e) are watermarked F16 images by the method [7]. (c) and (f) are watermarked F16 images by COCOA algorithm.

Table 3
PSNR summary of COCOA watermarked color images before and after median filtering.

Image	Logo pattern	PSNR value (dB)					
		Method [7]			COCOA method		
		Before	After	After (wm)	Before	After	After (wm)
Lena	NCTU	27.0	21.2	24.7	31.6	23.1	24.5
Baboon	NCTU	27.1	17.7	19.4	30.2	18.5	19.9
F16	NCTU	28.8	21.8	23.1	31.6	22.5	23.3
Lena	IIM	26.8	21.3	24.7	32.7	23.3	24.7
Baboon	IIM	27.2	17.8	19.4	31.0	18.5	19.9
F16	IIM	28.1	21.9	23.2	32.4	22.5	23.5

Even when we are encouraged by the simulation outcomes, we are fully aware that subsequent signal processing operations like equalization, sharpening or background texturizing could elude the viewers by adjusting the watermark visual effect, but such study is beyond the discussion in this research. However, it is apparent that a huge amount of labour and human intervention is inevitable for the current removal attacks. At the present time, COCOA watermarking technique can resist both image recovery and watermark removal attacks from the simulation results.

In summary, after intensive performance comparisons, the proposed COCOA algorithm not only provides high PSNR values for watermarked images, but also produces high robustness for attacks. Therefore, we are convinced that the proposed content and contrast aware COCOA approach with the consideration of the Human Visual System model for visible watermarking is a superior scheme among the referred published techniques.

5. Discussion and future researches

There are several issues and future research directions that the authors would like to address in this session on COCOA algorithm.

5.1. Complexity of COCOA with the Human Vision System

The computation complexity of COCOA with the Human Vision System is low from the view of mathematical analysis. The whole complexity should be discussed for wavelet transform, CSF and NVF calculation, respectively.

Suppose the synthesis filters are h (low-pass) and g (high-pass) for wavelet transform. Take $|h| = 2N$, $|g| = 2M$, and assume $M \geqslant N$. The cost of the standard algorithm for CDF 9/7 filters [25] is $4(N + M) + 2$ and could be sped up by the lifting algorithm in [30] to $2(N + M + 2)$. The computation of wavelet transform is linear time mathematics.

On the other hand, CSF masking is employed to apply the CSF in the DWT domain, and the associated perceptual weighting function can be pre-calculated for each subband as shown in Fig. 2(b). Therefore, the complexity of CSF implementation in COCOA becomes the coefficient multiplication from the look-up table. This can be efficiently done in linear-time.

Regarding the complexity of NVF, $\eta(\gamma)$ and gamma function can be pre-calculated by the look-up table when the shape parameter is decided. $r(i, j)$ in Eq. (6) is determined by the local means and the local variance which are related to the window size. The complex-

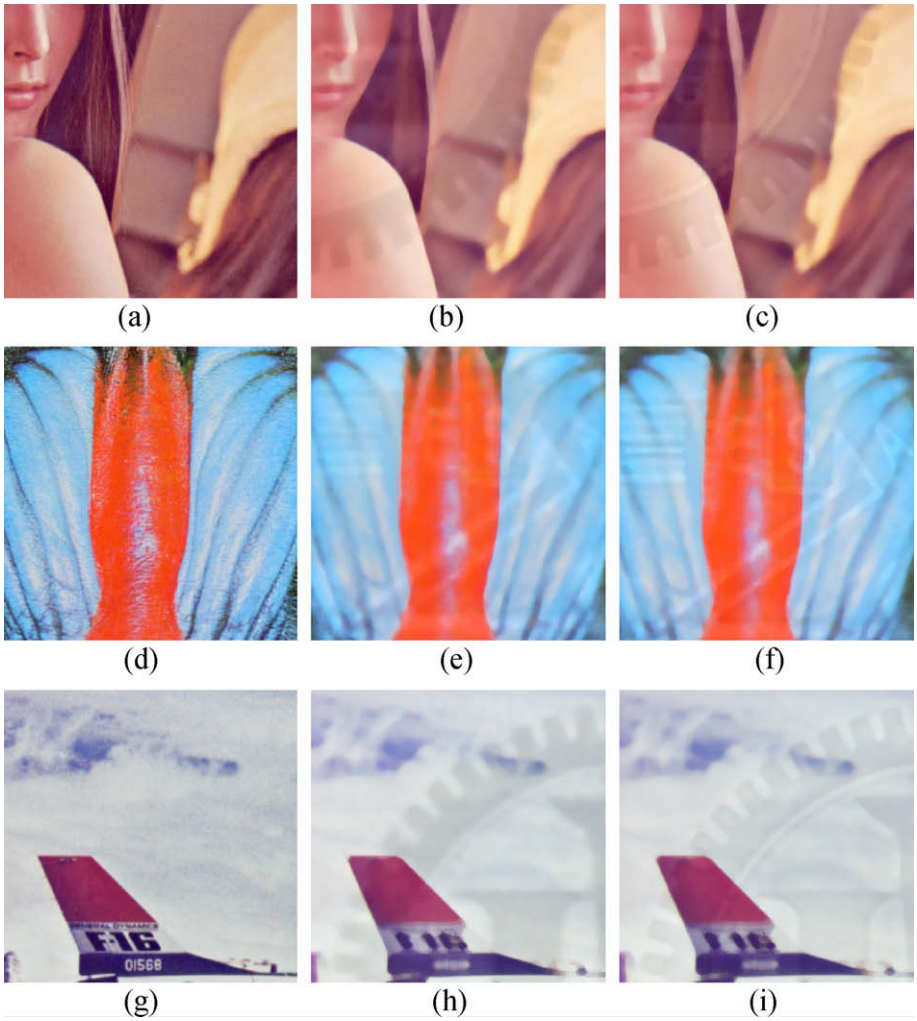

Fig. 10. The visual quality comparison of close-ups for 7 × 7 median filtering attack for Lena, Baboon and F16 images. (a), (d) and (g) are close-ups of Fig. 5(a, d and g). (b), (e) and (h) are watermarked images by the method [7] after filtering. (c), (f) and (i) are watermarked images by COCOA algorithm after filtering.

Table 4
PSNR summary of COCOA watermarked color images before and after JPEG2000 compression.

Image	Logo pattern	PSNR value (dB)					
		Method [7]			COCOA method		
		Before	After	After (wm)	Before	After	After (wm)
Lena	NCTU	27.0	26.0	34.5	31.6	29.3	34.0
Baboon	NCTU	27.1	23.0	26.1	30.2	24.1	26.5
F16	NCTU	28.8	27.8	34.6	31.6	29.7	34.4
Lena	IIM	26.8	25.9	34.7	32.7	29.8	34.5
Baboon	IIM	27.2	23.0	26.1	31.0	24.2	26.6
F16	IIM	28.1	27.0	35.0	32.4	30.2	35.3

ity of local means and variance is $O(l^2)$, when l ($=2L+1$) is the window size. In this study, the window size for $L = 1$ is 3×3. Besides, the global variance is obtained for each wavelet subband, and there are 15 subbands after 5 level wavelet decomposition. The total amount of calculation approximately equals to the image size (we can use static array to store the results). Thus, global variance takes $O(n^2)$ computation and the overall time complexity for NVF is no more than $O(n^2)$ ($O(n^2 \cdot l^2 + n^2) \approx O(n^2)$), since image width n is much larger than l.

From our simulation, the visible watermark embedding process of COCOA under Intel Pentium 3.2G Hz, 1G RAM will need less than 0.5 seconds to complete for 512×512 testing images. In conclusion, results from the mathematical analysis and simulation show that the COCOA complexity is low and suitable for practical applications.

5.2. The collaboration of visible and invisible watermarking for COCOA

Future research on COCOA will need to focus on the collaboration of visible and invisible watermarking [4–6,31,32] which can be used for content authentication and temper detection. The content authentication schemes which are based on digital watermarking is classified as watermarking-based authentication scheme [4,5,33]. The fragile and semi-fragile watermarks can be

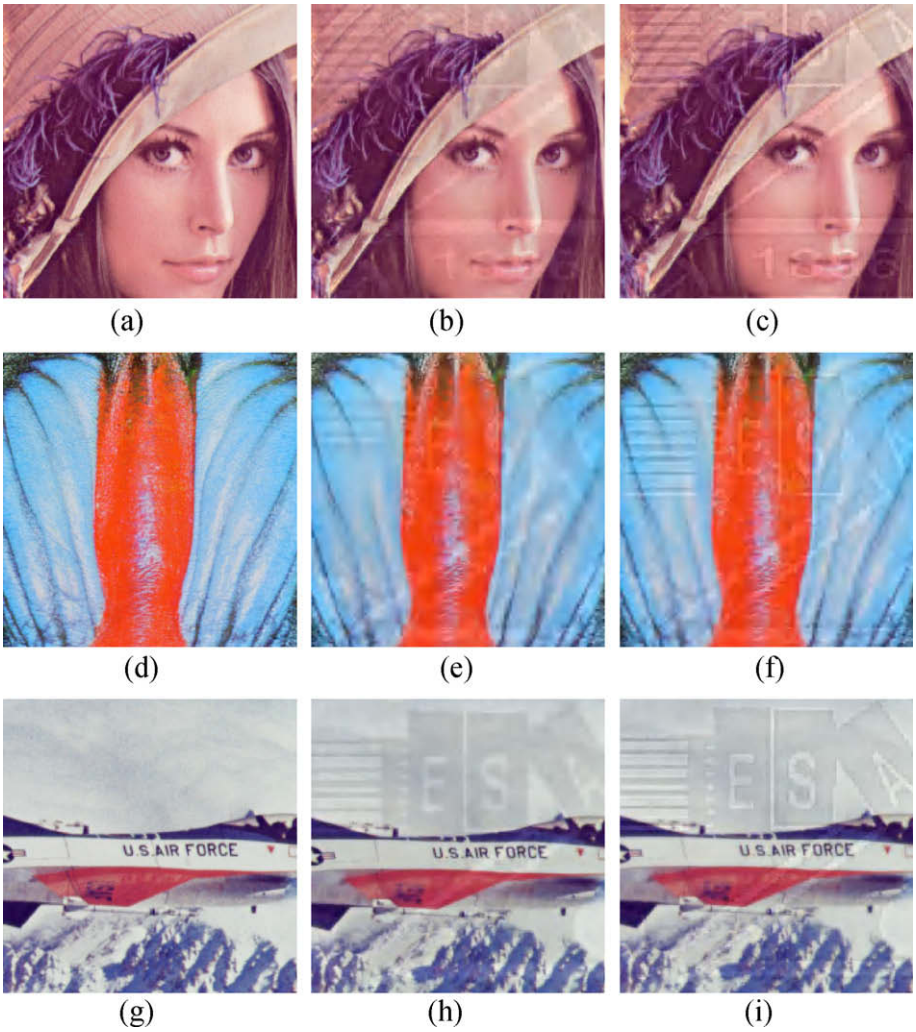

Fig. 11. The visual quality comparison of close-ups for JPEG2000 compression attack for Lena, Baboon and F16 images. (a), (d) and (g) are close-ups of Fig. 4(a, d and g). (b), (e) and (h) are watermarked images by the method [7] after compression. (c), (f) and (i) are watermarked images by COCOA algorithm after compression.

embedded in the spatial domain or the transformed domain for COCOA. However, the schemes that embed watermark in the transformed domain offer a higher degree of robustness [1]. In [34], the authors presented a fragile watermarking scheme for the authenticating region of interest (ROI) of the image. The reference mask is first obtained by Poisson matting, and the watermark is embedded according to the reference mask which represents the region of interest of the image. On the other hand, by utilizing the least significant bit (LSB) of data, we find the schemes using the spatial domain are simpler than the ones using transform domain. Fragile watermarking techniques [33] for content authentication are usually based on the concept of checksum produced by the secure hash functions (e.g. MD5, SHA160) to verify the completeness of an image. The approaches can detect and localize tampered region correctly, but they treat admissible manipulations such as JPEG compression and channel AWGN as malicious attacks. Therefore, fragile watermarks are less practical than semi-fragile watermarks.

As for semi-fragile watermarking schemes [32,35,36], they have been applied to verify the integrity of digital contents and tolerate a certain degree of mild modifications. For example, Ding et al. [36] propose a wavelet-based chaotic semi-fragile watermarking scheme based on chaotic map and odd–even quantization. Their scheme can detect and localize malicious attacks with the high peak signal-to-noise ratio (PSNR), while allowing more JPEG compression and channel additive white Gaussian noise (AWGN) tolerance.

5.3. The study of watermark removal techniques

Even when the authors are essentially working on the watermark design studies, it is still fundamental to understand all the possible techniques applied to remove the watermarks, such as image-inpainting and ICA. Understanding how the removal techniques will help the authors to design more robust watermarking methods. We believe that the study of watermarking design and watermark removal attacks make up an endless research cycle. These research efforts will in the end benefit all consumers and copyright owners in digital rights management (DRM).

5.4. The study of perceptual based image quality assessment for visible watermarking

It is crucial and necessary to examine the objective criteria for the evaluation of image quality for different visible watermark techniques that are based on models of visual perception. HVS quality measures generally need subjective quality scores based on controlled environment like viewing distance and display resolution. Although such studies are beyond the scope of our research

Fig. 12. Recovering the COCOA watermarked images by using ICA based technique [23]. (a) Watermarked Lena image with NCTU logo. (b) Recovered image of (a). (c) Watermarked Lena image with IIM logo. (d) Recovered image of (c).

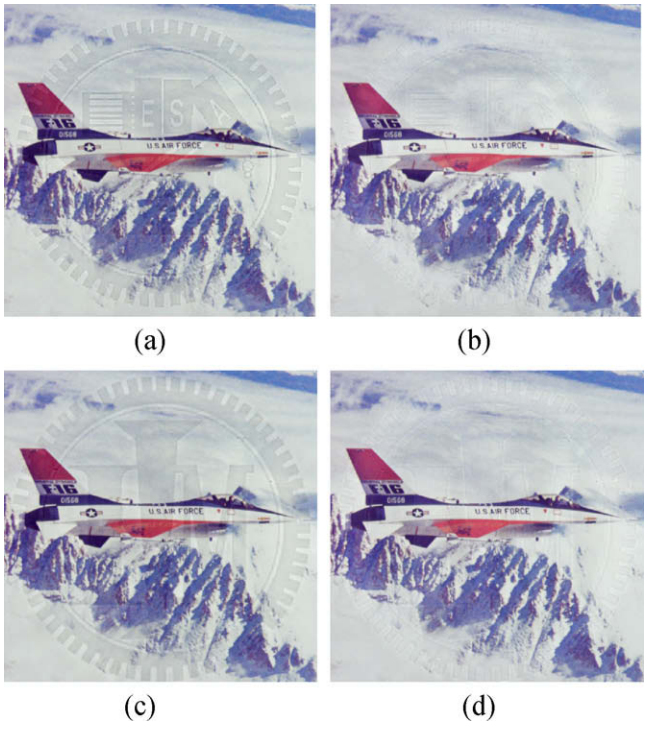

Fig. 14. Recovering the COCOA watermarked images by using ICA based technique [23]. (a) Watermarked F16 image with NCTU logo. (b) Recovered image of (a). (c) Watermarked F16 image with IIM logo. (d) Recovered image of (c).

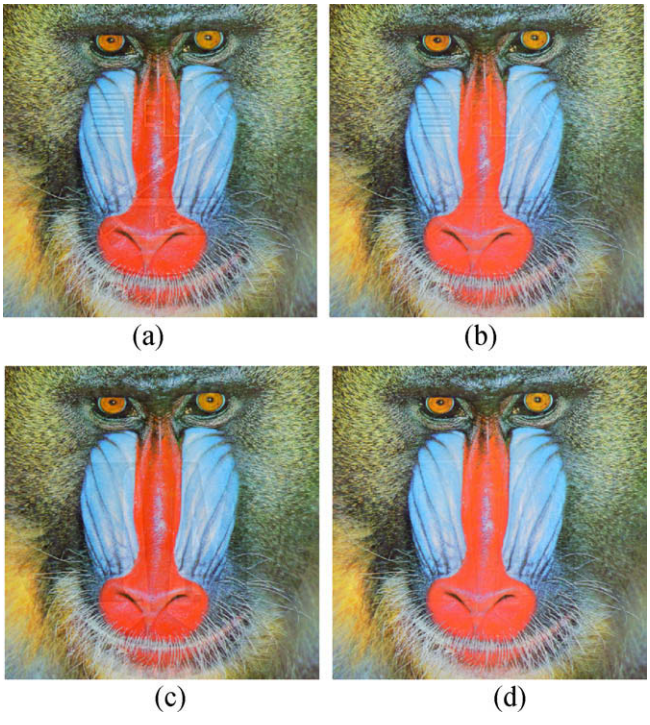

Fig. 13. Recovering the COCOA watermarked images by using ICA based technique [23]. (a) Watermarked Baboon image with NCTU logo. (b) Recovered image of (a). (c) Watermarked Baboon image with IIM logo. (d) Recovered image of (c).

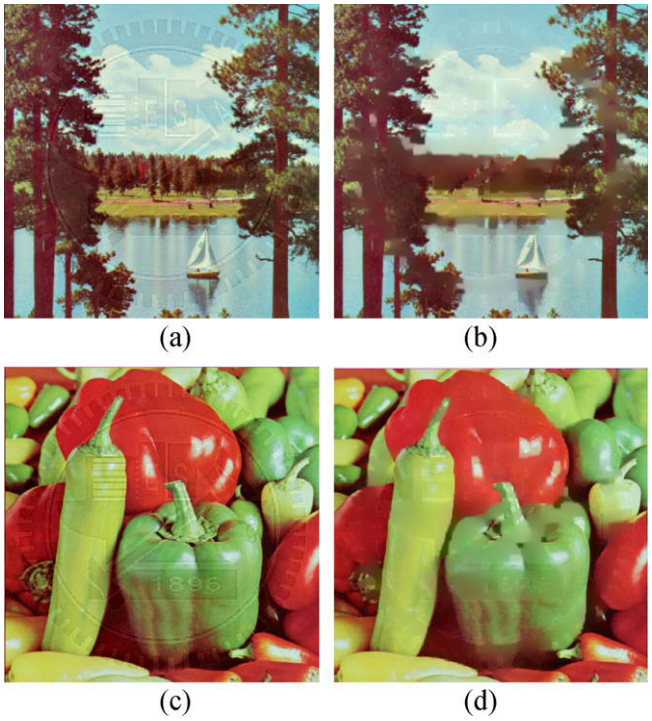

Fig. 15. Recovering the watermarked images by using image-inpainting based technique [22]. (a) COCOA watermarked Boat image with NCTU logo. (b) Recovered image of (a). (c) COCOA watermarked Peppers image with NCTU logo. (d) Recovered image of (c).

here, this topic has attracted wide academic and industry studies. For example, the near-threshold perceptual metrics [20,37–39] have been developed over the last decade. Such metrics have explicitly accounted for the Human Visual System sensitivity to noise by estimating thresholds above which distortion is just-noticeable, and can successfully account for the spatial and temporal frequency sensitivity of the eye, and the contrast and luminance

masking. Another class of metrics that has received a lot of attention, recently, is that of the structural similarity metrics [40]. MSE and traditional perceptual metrics are quite sensitive to spatial shifts, intensity shifts, contrast changes, and scale changes. In contrast, the structural similarity SSIM [41–43] metrics model perception implicitly by taking into account the fact that the HVS is adapted for extracting structural information (relative spatial covariance) from images. In brief, the perceptual based image quality assessment for visible watermarking deserves further investigation as future studies.

In summary, the complexity of COCOA is rather low for practical use. Those fragile or semi-fragile watermarking techniques can be adopted in COCOA to create the content authentication and temper detection tools. The understanding of watermark removal and image recovery techniques will help the design of the watermarking researches. In addition, the perceptual based image quality assessment for visible watermarking is necessary for future studies. However, in order to make the complete system secure, we believe an effective and robust visible watermarking scheme is necessary as the first priority for digital rights protection. Therefore, the visible watermarking scheme of COCOA proposed in this study has proved its capability to resist the intentional attacks, its integration with other methods could extend its usability and functional versatility for practical use.

6. Conclusion

In this study, we have proposed a novel visible watermarking technique based on the content and contrast aware approaches with the consideration of a Human Visual System model called COCOA. The intensity of the watermark in different regions of the image depends on the underlying content of the image and humans' sensitivity to spatial frequencies. The collaboration of CSF and NVF for the HVS model is leveraged with the noise reduction of the visibility thresholds for HVS in the DWT domain. The perceptual weights are fine tuned for watermark embedding which results significant improvement over the watermarked images by the method solely based on CSF regarding the image quality, translucence and robustness of the watermarking. After the intensive performance comparison, the experimental results demonstrate that COCOA technique not only provides the watermarked images with high PSNR values and better image fidelity, but also improves the robustness against various signal processing and advanced watermark removal attacks. In conclusion, with its robustness resisting attacks, the COCOA visible watermarking provides an instant recognition of the copyrights of multimedia data in a more active way. In addition, COCOA can even adopt the fragile or semi-fragile watermarking techniques to create the content authentication and temper detection applications, which can extend its usability and functional versatility for practical use.

Acknowledgments

The author would like to thank Prof. Soo-Chang Pei and Dr. Yi-Chong Zeng for valuable suggestion. Special thanks for Dr. Yi-Chong Zeng who verifies the ICA watermark recovery simulation comparison for this study.

The author would like to thank the anonymous reviewers with their valuable comments to improve the quality of this manuscript and Chih-Wen Lin at National Chiao Tung University who helps to write the programs and Matlab scripts for software experiments.

This work is supported by the National Science Council in Taiwan, Republic of China, under Grant NSC95-2416-H009-027, NSC96-2416-H009-015 and NSC97-2410-H009-034.

References

[1] I.J. Cox, J. Kilian, J.F.T. Leighton, T. Shamoon, Secure spread spectrum watermarking for multimedia, IEEE Trans. Image Proc. 6 (12) (1997) 1673–1687.
[2] S.J. Lee, S.H. Jung, A Survey of watermarking techniques, IEEE Int'l Symposium on Industrial Electronics, 2001, 272–277.
[3] G.W. Braudaway, K.A. Magerlein, F.C. Mintzer, Protecting publicly available images with a visible image watermark, Proc. SPIE, Int. Conf. Electron. Imaging 2659 (1996) 126–132.
[4] D. Kundur, C.Y. Lin, B. Macq, H. Yu, Special issue on enabling security technologies for digital rights management, Proc. IEEE (2004) 879–882.
[5] C.S. Lu, H.Y.M. Liao, Multipurpose watermarking for image authentication and protection, IEEE Trans. Image Proc. 10 (10) (2001) 579–1592.
[6] D. Yu, F. Sattar, K.K. Ma, Watermark detection and extraction using independent component analysis method, EURASIP J. Appl. Signal Process. 1 (2002) 92–104.
[7] B.B. Huang, S.X. Tang, A contrast-sensitive visible watermarking scheme, IEEE Multimedia 13 (2) (2006) 0–66.
[8] J. Meng, S.F. Chang, Embedding visible video watermarks in the compressed domain Proc, ICIP 1 (1998) 474–477.
[9] S.P. Mohanty, K.R. Ramakrishnan, M.S. Kankanhalli, A dual watermarking technique for image, Proc. 7th ACM Int. Multimedia Conf. 2 (1999) 9–51.
[10] P.M. Chen, A visible watermarking mechanism using a statistic approach, Proc. 5th Int. Conf. Signal Process. 2 (2000) 910–913.
[11] M.S. Kankanhalli, R. Lil, R. Ramakrishnan, Adaptive visible watermarking of images, Proc. IEEE Int'l Conf. Multimedia Comput. Syst. (1999) 68–73.
[12] S.P. Mohanty, M.S. Kankanhalli, R. Ramakrishnan, A DCT domain visible watermarking technique for image, Proc. IEEE Int. Conf Multimedia Expo 20 (2000) 1029–1032.
[13] Y. Hu, S. Kwong, Wavelet domain adaptive visible watermarking, Electron. Lett 37 (20) (2001) 1219–1220.
[14] Y. Hu, S. Kwong, An image fusion-based visible watermarking algorithm, in: Proc. Int'l Symp. Circuits Syst., IEEE Press, 2003, pp. 25–28.
[15] L. Yong, L.Z. Cheng, Y. Wu, Z.H. Xu, Translucent digital watermark based on wavelets and error-correct code, Chinese J. Comput. 27 (11) (2004) 533–1539.
[16] J.L. Mannos, D.J. Sakrison, The effects of a visual fidelity criterion on the encoding of images, IEEE Trans. Info. Theory 20 (4) (1974) 25–536.
[17] D. Levický, P. Foris, Human Visual System Models in Digital Image Watermarking, Radio Eng. 13 (4) (2004) 38–43.
[18] A.P. Beegan, L.R. Iyer, A.E. Bell, Design and evaluation of perceptual masks for wavelet image compression, in: Proc. 10th IEEE Digital Signal Processing Workshop, 2002, pp. 88–93.
[19] S. Voloshynovskiy, et al., A stochastic approach to content adaptive digital image watermarking, in: Proc. 3rd Int. Workshop Information Hiding, Dresden, Germany, 1999, pp. 211–236.
[20] A.B. Watson, G.Y. Yang, J.A. Solomon, J. Villasenor, Visibility of wavelet quantization noise, IEEE Trans. Image Proc. 6 (8) (1997) 1164–1175.
[21] M. Bertalmio, V. Caselles, C. Ballester, Image inpainting, SIGGRAPH 2000, August 2000.
[22] C.H. Huang, J.L. Wu, Attacking visible watermarking schemes, IEEE Trans. Multimedia 6 (1) (2004) 16–30.
[23] S.C. Pei, Y.C. Zeng, A novel image recovery algorithm for visible watermarked image, IEEE Trans. Inform. Forensics Secur. 1 (4) (2006) 543–550.
[24] M.J. Tsai, C.W. Lin, The collaboration of noise reduction and human vision system models for a visible watermarking algorithm, IEEE Int. Conf. Image Process. 3 (2007) 273–276.
[25] J.D. Villasenor, B. Belzer, J. Liao, Wavelet filter evaluation for image compression, IEEE Trans. Image Process. 4 (8) (1995) 053–1060.
[26] USC SIPI—The USC-SIPI Image Database. Available from: <http://sipi.usc.edu/services/database/Database.html>.
[27] AiS Watermark Pictures Protector. Available from: <http://www.watermarker.com>.
[28] StirMark. Available from: <http://www.petitcolas.net/fabien/software/StirMarkBenchmark_4_0_129.zip>.
[29] JPEG2000 compression. Available from: <http://www.ece.uvic.ca/~mdadams/jasper/>.
[30] I. Daubechies, W. Sweldens, Factoring wavelet transforms into lifting steps, J. Fourier Anal. Appl. 4 (3) (1998) 247–269.
[31] C. Rey, J.L. Dugelay, A survey of watermarking algorithms for image authentication, EURASIP J. Appl. Signal Process. 6 (2002) 613–621.
[32] C. Fei, D. Kundur, R. Kwong, Analysis and design of secure watermark-based authentication systems, IEEE Trans. Inform. Forensics Secur. 1 (2006) 43–55.
[33] C.C. Chang, Y.S. Hu, T.C. Lu, A watermarking-based image ownership and tampering authentication scheme, Pattern Recogn. Lett. 27 (5) (2005) 39–446.
[34] Y. Chu, Y. Zhang, S. Zhang, X. Ye, Region of interest fragile watermarking for image authentication, in: First International Multi-Symposiums on Computer and Computational Sciences, vol. 1, 2006, pp. 726-731.
[35] D. Zou, Y.Q. Shi, Z. Ni, W. Su, A semi-fragile lossless digital watermarking Scheme based on integer wavelet transform, IEEE Trans. Circuits Syst. Video Technol. 16 (10) (2006) 1294–1300.
[36] K. Ding, C. He, L.G. Jiang, H.X. Wang, Wavelet-based semi-fragile watermarking with tamper detection, IEICE Trans. Fundam. Electron. Commun. Comput. Sci. E88-A (3) (2005) 87–790.

[37] A.B. Watson, Toward a perceptual video quality metric, in: HVEI 1998 Proceedings, 1998, pp. 139–147.
[38] A.B. Watson, DCT quantization matrices visually optimized for individual images, Proc. SPIE 1913 (1993) 202–216.
[39] P.C. Teo, D.J. Heeger, Perceptual image distortion, Proc. SPIE 2179 (1994) 127–141.
[40] Z. Wang, A.C. Bovik, H.R. Sheikh, E.P. Simoncelli, Image quality assessment: from error visibility to structural similarity, IEEE Trans. Image Process. 13 (4) (2004) 600–612.
[41] N. Bekkat, A. Saadane, Coded image quality assessment based on a new contrast masking model, J. Electron. Imaging 13 (2004) 341–348.
[42] Z. Wang, E.P. Simoncelli, An adaptive linear system framework for image distortion analysis, IEEE Int. Conf. Image Process 2005 (3) (2005) 1160–1163.
[43] A.C. Brooks, X.N. Zhao, T.N. Pappas, Structural similarity quality metrics in a coding context: exploring the space of realistic distortions, IEEE Trans. Image Process. 17 (8) (2008) 1261–1273.